

Article

An Efficient Approach for Nitrogen Diffusion and Surface Nitriding of Boron-Titanium Modified Stainless Steel Alloy for Biomedical Applications

Sadaqat Ali ^{1,2,*} , Ahmad Majdi Abdul Rani ^{1,*}, Riaz Ahmad Mufti ^{2,*}, Sri Hastuty ³, Murid Hussain ⁴, Nasir Shehzad ⁴, Zeeshan Baig ⁵ and Abdul Azeez Abdu Aliyu ⁶

¹ Mechanical Engineering Department, Universiti Teknologi PETRONAS (UTP), Bandar Seri Iskandar, Perak 32610, Malaysia

² School of Mechanical & Manufacturing Engineering, National University of Sciences and Technology (NUST), H-12, Islamabad 44000, Pakistan

³ Mechanical Engineering Department, Universitas PERTAMINA, Jakarta 12220, Indonesia

⁴ Department of Chemical Engineering, COMSATS University, Lahore campus, Lahore 54000, Pakistan

⁵ Centre of Excellence in Science & Applied Technologies, Islamabad 44000, Pakistan

⁶ Department of Mechanical Engineering, Bayero University Kano, 700241 Kano, Nigeria

* Correspondence: engineersadaqat@gmail.com (S.A.); majdi@utp.edu.my (A.M.A.R.); riazmufti@smme.nust.edu.pk (R.A.M.); Tel.: +92-333-9410290 (S.A.); +60-5368-7155 (A.M.A.R.); +92-519086-6055 (R.A.M.)

Received: 12 June 2019; Accepted: 2 July 2019; Published: 5 July 2019



Abstract: Austenitic 316L stainless steel has been the most widely acceptable biomaterial for producing implants. The downside of this material includes the leaching of nickel ions from the matrix that limits its' usage in implant manufacturing. In this research, production of stainless steel alloy modified with boron and titanium is investigated. The sintering of the alloy systems is carried out in nitrogen atmosphere for a dwell time of 8 h. The X-Ray diffraction (XRD) analysis reveals that dwell time and alloy composition leads to the formation of strong nitrides and borides. The X-Ray Photoelectron Spectroscopy (XPS) results show the presence of nitrogen on to the surface of sintered specimens. The nitride layer on the surface of the specimens is helpful in the retention of nickel ions in the stainless steel matrix, as indicated in the weight loss measurements. The cytotoxicity assessment indicates that the developed alloys are biocompatible and can be used as implant materials.

Keywords: implant; stainless steel; nickel; leaching; nitrogen; cytotoxicity

1. Introduction

Among the commercially available biomaterials, stainless steel (SS) has been the material of choice since the 1930s, when the first hip replacement was carried out for orthopedic patient using a stainless steel material [1,2]. Since then, this material has gained an incredible attention due to its cheaper cost, adequate mechanical properties, and biocompatibility [3,4]. In 1926, Strauss discovered 316L type stainless steel, which became used in surgical procedures [5]. It contains chromium and nickel (18 wt.% and 8–12 wt.% respectively) along with molybdenum and a very low amount of carbon. The presence of at least 12 wt.% of chromium in the stainless steel matrix makes it resistant to rust and hence gives it the quality of being stainless. The chromium also combines with oxygen in the atmosphere to develop a thin passive layer of chromium oxide. The oxide layer along with other elements present in the matrix enhances corrosion resistance of this type of steel and makes it a better choice among other biomaterials. The implants manufactured from 316L SS possess an adequate strength and ease of

fabrication at a very low cost as compared to titanium, cobalt chromium, and other materials of this class [6–8].

In 316L stainless steel, the nickel has been added to promote the austenitic structure of this material [9]. However, it has been reported that this material is subjected to localized corrosion when used as an implant material [10,11]. The implant gets corroded in the human body and releases nickel, iron, and chromium ions [12]. The pervasiveness of sensitivity to metals and their ions in humans is around 10% to 15%. Among various materials, nickel sensitivity has the most pervasiveness, with approximately 14% [13,14]. Among the released ions, nickel has been reported to be the cause of mutagenic and genotoxic activities in human tissues [15]. Nickel has also been reported to be the main cause of contact allergy when it is in contact with the skin of patients [15,16]. The allergic reaction in patients was firstly reported in 1966 when an orthopedic implant was noticed with eczematous rash and dermatitis [17,18]. Similar observations with allergic reactions have been reported in patients owing mostly to skin diseases, swelling of that particular area, discomfort, and erythema [19–21]. The release of nickel and other metal ions from implants is emphatically associated with poor corrosion resistance in human physiological conditions [22–24]. This leaching of ions and poor corrosion resistance necessitates the need for modifying the 316L stainless steel matrix by alloying with additives and improving the surface of the implants [25,26]. In this framework, adding boron and titanium in a stainless steel matrix has been introduced to enhance the corrosion resistance of the resulting stainless steel alloy, along with controlling the leaching of ions from the stainless steel matrix by optimizing the sintering parameters. The elemental boron can improve the sinter ability of the alloy system as it is an active sintering additive for stainless steel and increasing the overall densification process [27,28]. Boron also possesses a good tendency of forming borides with iron and nickel that can decrease the leaching of nickel ions from the stainless steel matrix [29]. Pure titanium has attracted much attention as a potential biomaterial owing to its exceptional corrosion resistance and mechanical properties among the available biomaterials [30,31]. However, like any other material used in physiological conditions of the human body, it is subjected to biological factors that can harm the survival of implant, leading to early failures [32,33]. In this regard, pure titanium has been alloyed with other elements to develop alloys that can fulfil the clinical demands for the manufacturing of implants [34]. Both of these alloying elements can address the highlighted issues related to use of stainless steel alloy as an implant material. Nitrogen is an effective stabilizer of austenitic structure and increased corrosion resistance [16]. Nitrogen containing stainless steels have high work-hardening rates in addition to increased strength as compared to conventional steel [35,36]. The sintering of stainless steel alloy in nitrogen has been proven to improve the densification process along with improved mechanical properties [37].

In this study, sintering of the alloys is carried out in nitrogen atmosphere. The dwell time of 8 h has been selected for maximum diffusion of nitrogen into the matrix. The formation of institutional and substitutional elements like chromium nitride, iron nitride and carbon nitride may contribute to the strengthening of the alloy systems [38]. The sintering parameters are likely to develop a nitride layer on the surface of the alloy, thereby forming a passive layer to minimize the leaching of nickel and other ions from the matrix.

2. Materials and Methods

2.1. Specimen Preparation

The pure 316L stainless steel powder was used as the matrix to prepare the specimens. The chemical composition of the 316L SS powder is shown in Table 1. In this study, five different formulations have been developed, as shown in Table 2. The first formulation is pure 316L stainless steel whereas the other four have been modified with boron and titanium. The amount of boron used is 0.25 wt.% for titanium containing samples, whereas the amount of titanium addition is varied from 0.5 to 2 wt.%.

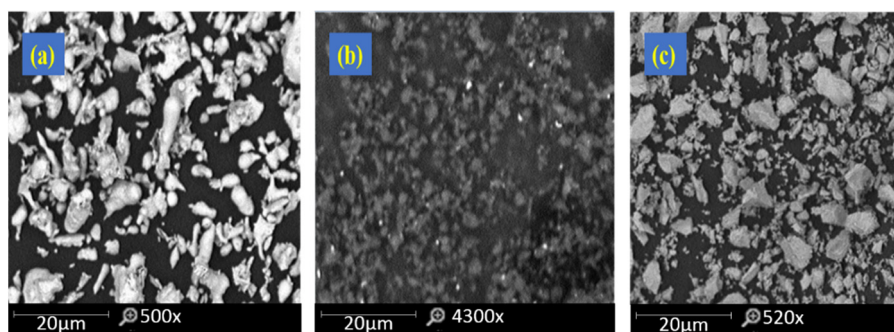
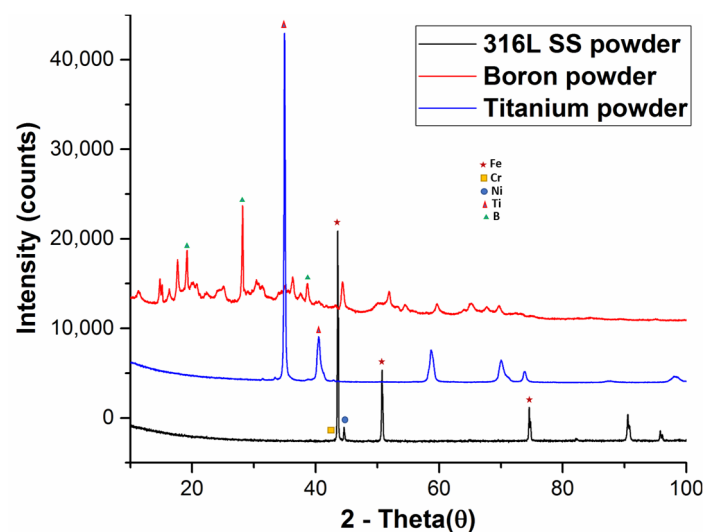
Table 1. Chemical composition of 316L SS powder.

Element	C	Si	O	Mn	Ni	Cr	Mo	Fe
wt.%	0.028	0.9	0.068	1.5	12.01	17.04	2.4	Balance

Table 2. Composition of the alloy systems produced.

S.No	Alloy	Composition
1	S1	Pure 316L SS
2	S2	316L SS + 0.25 B + 0.5 Ti
3	S3	316L SS + 0.25 B + 1 Ti
4	S4	316L SS + 0.25 B + 1.5 Ti
5	S5	316L SS + 0.25 B + 2 Ti

The morphology of the powders used in this study was carried out using Scanning Electron Microscope (Phenom-Pro X, Dillenburgstraat 9T, The Netherlands) and XRD analysis was carried out using X-ray diffraction (X'Pert3 powder and Empyrean, PANalytical B.V, Lelyweg, Almelo, The Netherlands). The SEM images and XRD graph of all the powders used in the study have been shown in Figures 1 and 2 respectively. The powder mixtures were blended in turbula mixer for 8 h to get a uniformly dispersed powder combinations. The specimens from each powder combination were prepared by uniaxial cold compaction process. The specimens were made in the form of a disc with a 30 mm diameter and 4 mm thickness at a pressure of 800 MPa. The compacted samples were then sintered in a tube furnace at a temperature of 1200 °C under nitrogen atmosphere. The dwell time for all the samples was 8 h for a maximum diffusion of nitrogen into the samples.

**Figure 1.** SEM images of (a) 316L SS, (b) boron, (c) titanium powder.**Figure 2.** XRD spectra of powders used in this study.

2.2. Green and Sintered Density Measurement

The green and sintered densities of all specimens were measured using geometric method and Archimedes' principle respectively. For the geometric method, the diameter and thickness of compacted specimens was measured and green density calculated via dividing mass by volume of the measured specimens. The sintered density of all the specimens was calculated using water displacement method using Archimedes' principle.

2.3. Microstructure and Micro Hardness Measurement

The microstructures of all sintered specimens were observed through Optical microscope (Leica DM LM, Germany). The specimens were firstly grinded using silicon carbide grinding papers (600, 800, 1000, 1200 and 1500) followed by polishing using 3 μm , 1 μm and 0.1 μm diamond paste respectively. The samples were then etched using Carpenters stainless steel etchant before examining in the microscope. The elemental mapping of different elements present in the matrix was carried out using a Field Emission Scanning Electron microscope (FESEM, Model: VPFESM, Zeiss Supra55 VP, Oberkochen, Germany). The microhardness of sintered specimens was calculated using Vickers hardness tester (Leco LM 247AT, Lakeview Ave, St. Joseph, MI, USA). The testing is carried out by applying 200 gf and 15 s dwell time. At least five readings were taken for each specimen and the average micro hardness value was calculated.

2.4. Characterization of Sintered Specimens

The XRD analyses of all sintered specimens were done using X-ray diffractometer for the occurrence of compounds present in the matrix using scan range of 10–90° using X-ray diffractometer (X'Pert3 powder and Empyrean, PANalytical, B.V, Lelyweg, Almelo, The Netherlands). The XPS analyses was carried out using X-Ray photoelectron spectrometer (Thermo scientific, K-alpha, East Grinstead, UK) for investigation of elemental mass percentages of each element present on the sample surface.

2.5. Immersion Testing

The corrosion resistance of specimens was carried out through a weight loss method. The specimens were immersed for 28 days in artificial saliva solution to investigate the weight loss incurred. The artificial saliva solution was prepared as prescribed in the literature and had a composition of Urea (1.0 g/L), KCl (0.4 g/L), NaCl (0.4 g/L), $\text{Na}_2\text{S}\cdot 9\text{H}_2\text{O}$ (0.005 g/L), $\text{NaH}_2\text{PO}_4\cdot \text{H}_2\text{O}$ (0.69 g/L) and $\text{CaCl}_2\cdot 2\text{H}_2\text{O}$ (0.795 g/L) to adjust it to natural saliva composition [39,40]. The pH of prepared solution was observed to be 5.5 and in correspondence to pH of natural saliva. The weight of all the specimens was measured before and after immersion. After 28 days, each specimen was weighed again after cleaning to analyze the weight loss that incurred during the immersion period. The artificial saliva solution from each immersed specimen was analyzed for possible ions released using atomic absorption spectroscopy (Model: GTA120 Graphite Tube Atomizer supplied by Agilent, Stevens Creek Blvd, Santa Clara, CA, USA).

2.6. Cytotoxicity Assessment

The cytotoxicity assessment of all the specimens was conducted through cell cultures by using fibroblast cell line (NIH/3T3 ATCC[®] CRL-1658[™]) supplied by ATCC, Manassas, VA, USA. Using Dulbecco's Modified Eagle's Medium (DMEM), NIH/3T3 cells were expanded in the media that involved 100 $\mu\text{g}/\text{mL}$ of Pen/strep and 10 percent Fetal bovine serum (FBS) was augmented. The cells were expanded and grown to 90% confluency in an incubator at a temperature of 37 °C. The cells were then separated using trypsin–EDTA for seeding. The cells were counted with the help of microscope and hemacytometer on the seeding day. Around fifty thousand cells were sowed on each test specimen to check the compatibility of the NIH/3T3 cells with the specimens. The samples were diluted with the addition of 100 μL of the sample DMEM media into 1 mL before seeding. The cells were

cultured on tissue culture plastic plates deprived of specimens that were to be used as control. It was done to compare the values of DES specimens with the cultured cells. The sterilization of the specimens was performed using an ethanol solution. The sterilization was carried out for one hour, followed by rinsing with Phosphate buffer saline (PBS) for 15 min before seeding of the cells. The cells that were cultured without specimens were adopted as the controls (ISO 10993-5:2009). For the quantification of cell attachment and viability, fluorescent measurements of Alamar Blue were captured after three days. The PBS solution was used for rinsing of the cell seeded specimens. The specimens were later kept for incubation. Using a fluorescence plate reader, 3–4 h absorbance was calculated at 570 nm. The metabolic activity of cells took place and integrated an oxidation-reduction indicator. The indicator fluoresces as well as changes color. The fluorescence and change in color from blue (oxidized) to red (reduced) on the REDOX indicator is in response to the chemical reduction that takes place due to cell growth.

3. Results

3.1. Green and Sintered Density Measurements

The respective green and sintered densities of all specimens has been presented in Table 3. The green density of 316L SS specimens was 6.5 g/cm³ and its value keep on decreasing with increase of titanium addition. The decrease in green density is due to the diffusion of boron and titanium particles in the stainless steel matrix. Moreover, the density of titanium is also less than stainless steel and it reduced the green density. The sintering environment and dwell time resulted in improved densification. A densification of 95.88% is observed for 316L SS specimens, whereas a rate of 87.32% was observed for the 2 wt.% titanium added specimens. The table shows that the sintered density for all other specimens is low. This is due to the fact that the density of titanium is almost half of the 316L SS alloy. The boron addition had a major role in improving the densification process. Its addition maintained the sintered density of specimens nearby to the sintered density of pure 316L stainless steel specimens.

Table 3. Densities of all the specimens.

S.No	Alloy	Green Density	Sintered Density	Densification
1	S1	6.500 g/cm ³	7.575 g/cm ³	95.88%
2	S2	6.385 g/cm ³	7.387 g/cm ³	93.50%
3	S3	6.212 g/cm ³	7.139 g/cm ³	90.36%
4	S4	6.116 g/cm ³	7.008 g/cm ³	88.70%
5	S5	6.002 g/cm ³	6.899 g/cm ³	87.32%

3.2. Microstructure of Sintered Specimens

The microstructure of all the specimens was observed through optical microscope. The micrographs of the sintered specimens as viewed from optical microscope have been depicted in Figure 3. The elemental mapping of different elements present in the matrix for pure 316L stainless steel specimens and 2 wt.% titanium added specimens has been shown in the Figures 4 and 5, respectively. The maps confirmed the presence of nitrogen for pure and boron and titanium added 316L stainless steel specimens. This indicate that the sintering parameters helped in nitrogen diffusion into the matrix of stainless steel. It can be observed that the sintering environment and temperature had a notable effect on the microstructure of the specimens. The specimens were sintered properly with low porosity.

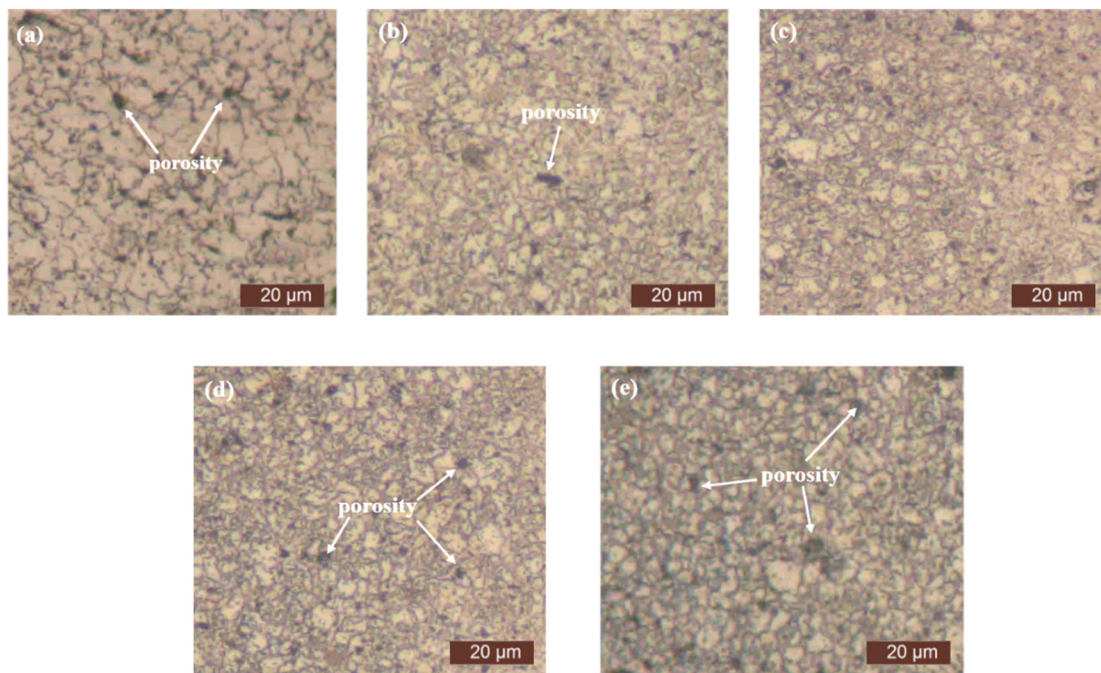


Figure 3. Microstructure of sintered samples (a) S1 (b) S2 (c) S3 (d) S4 (e) S5.

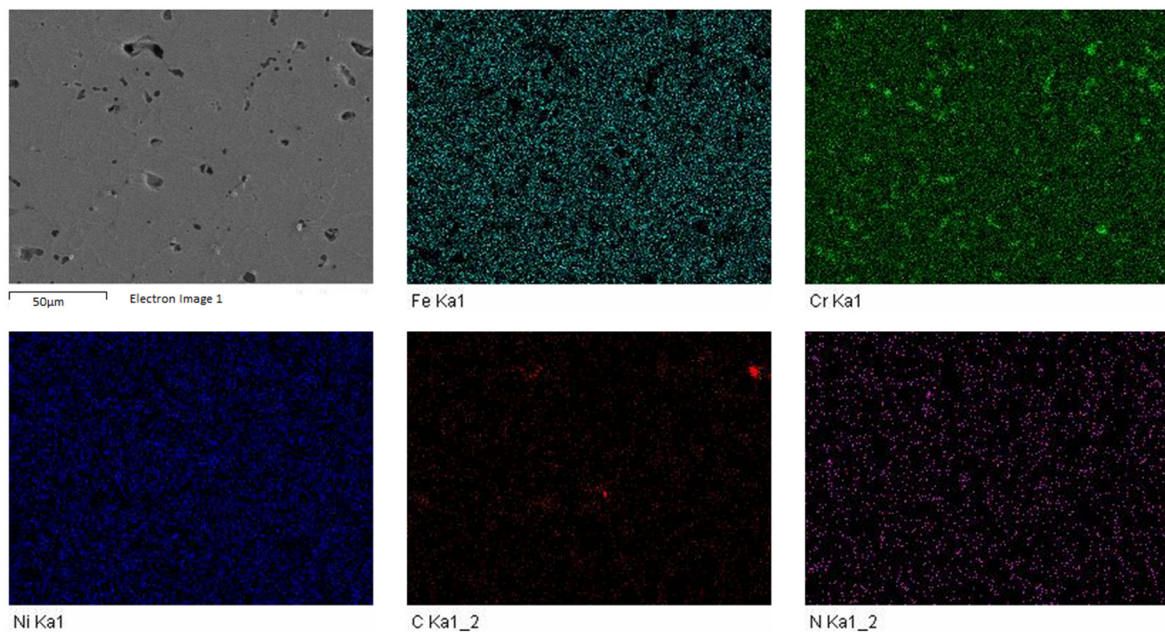


Figure 4. FESEM-EDS elemental maps for pure 316L stainless steel specimens.

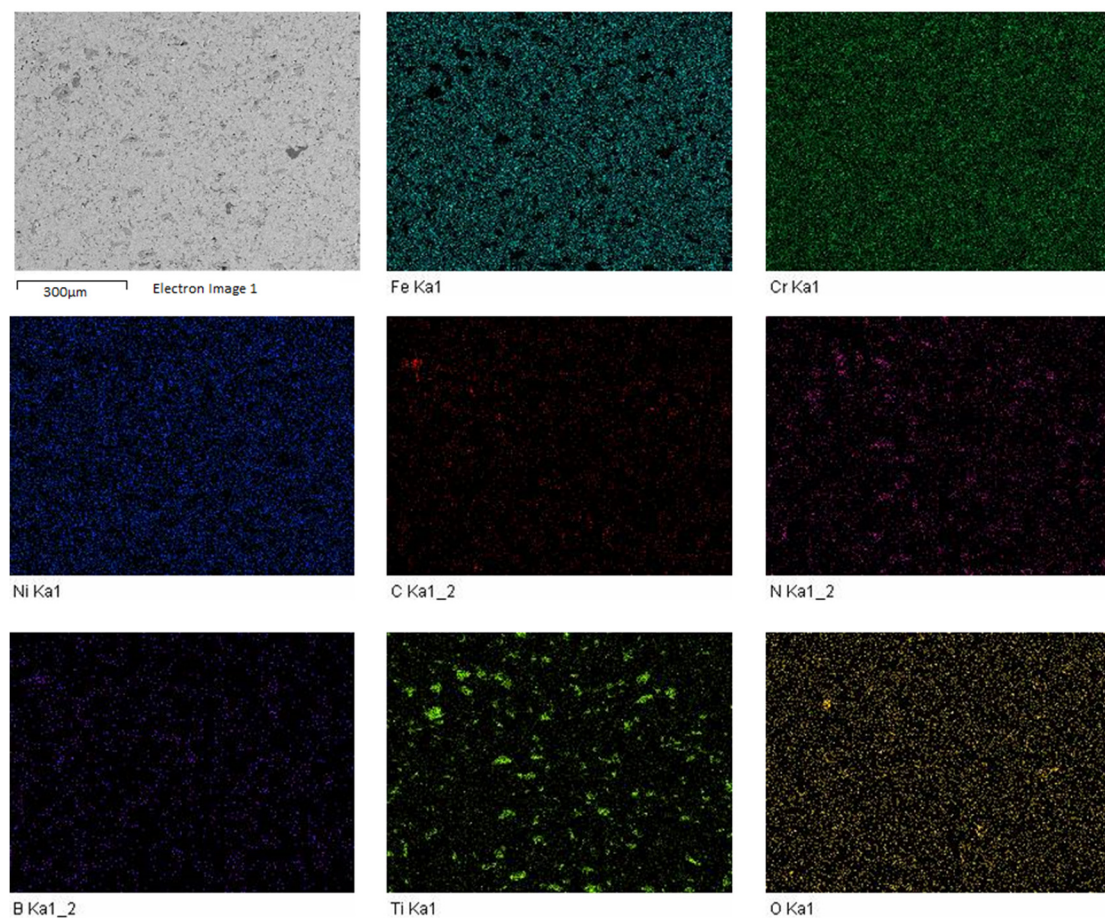


Figure 5. FESEM-EDS elemental maps for 2 wt.% titanium added 316L stainless steel specimens.

3.3. Micro Hardness of Specimens

The micro hardness of sintered specimens has been presented in Figure 6. The micro hardness of 316L stainless steel specimens was 235 HV. From Figure 6, it can be pointed out that micro hardness increases with an increasing titanium content. An enhancement in micro hardness was observed for all the specimens and a micro hardness of 366.6 HV was observed for specimens with 2 wt.% titanium addition. The increase in micro hardness value also is owed to the boron in the matrix that helped in increasing the micro hardness of the specimens produced.

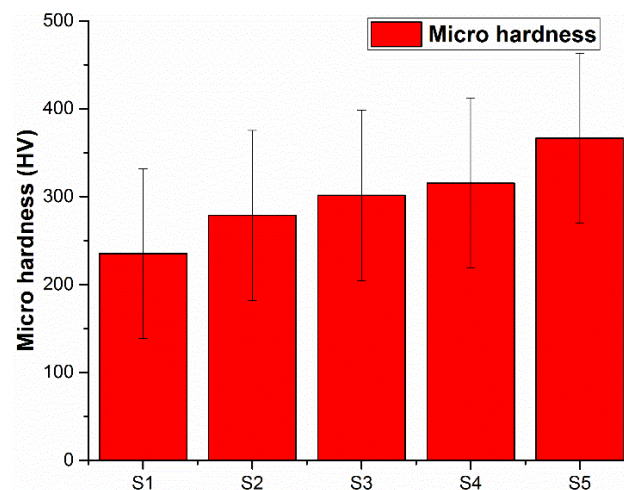


Figure 6. Micro hardness of all specimens.

3.4. XRD Analysis of Sintered Specimens

The XRD analysis was performed to investigate the occurrence of compounds present in the sintered alloy systems. The XRD patterns of all specimens have been shown in Figure 7. The results show the existence of austenitic structure (γ Fe) in all the specimens. The nitrogen has been diffused in all the samples, resulting in the formation of strong nitrides with carbon, iron, boron and titanium. The XRD pattern for pure 316 L SS specimen shows the formation of $\text{Ni}(\text{Cr}_2\text{O}_4)$ at d spacing of 2.49354 Å, C_3N_4 at d spacing of 2.51960 Å, Cr_2O_3 at d spacing of 2.66348 Å and $\text{FeN}_{0.324}$ at d spacing of 2.07500 Å. For the samples having 0.5 wt.% titanium, presence of NiTi at d spacing of 2.1191 Å, BN at d spacing of 3.33000 Å, Cr_2O_3 at d spacing of 2.66602 Å, $\text{FeN}_{0.0499}$ at d spacing of 43.469 Å and C_3N_2 at d spacing of 2.54500 Å was observed. The XRD results for 1 wt.% titanium added samples indicated the presence of $(\text{Cr}_{0.88}\text{Ti}_{0.12})\text{O}_3$ at d spacing of 2.67259 Å, $(\text{Fe}_{2.5}\text{Ti}_{0.5})_{1.04}\text{O}_4$ at d spacing of 2.54060 Å, Fe_2O_3 at d spacing of 1.68000 Å and $\text{FeN}_{0.0499}$ at d spacing of 2.08019 Å. In 1.5 wt.% titanium added samples, the following compounds were distinguished: $\text{TiN}_{0.90}$ at d spacing of 2.11900 Å, $(\text{Cr}_{0.88}\text{Ti}_{0.12})\text{O}_3$ at d spacing of 2.67259 Å and $\text{FeN}_{0.0560}$ at d spacing of 2.08366 Å. The identified compounds for 2 wt.% titanium added stainless steel samples were Cr_2O_3 at d spacing of 2.66602 Å, FeNi at d spacing of 2.07615 Å and BN at d spacing of 3.33000 Å.

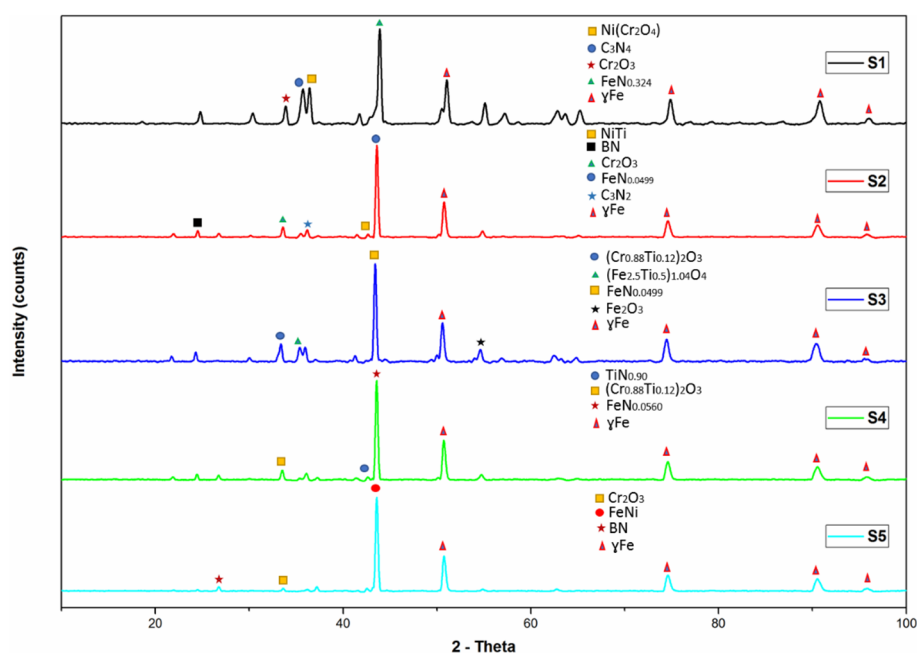


Figure 7. XRD spectra for all specimens.

3.5. XPS Analysis of Sintered Specimens

The X-Ray Photoelectron Spectroscopy (XPS) analysis was carried out to determine the different elements present on surface of the sintered specimens. The XPS spectra for all specimens have been shown in Figure 8. The analysis reveal the greatest percentage of oxygen present on the surface followed by iron and chromium. The oxygen reacted with chromium to form chromium oxide and with iron to form iron oxide. These oxide layers covered the outer surface of all specimens with a passive film of iron and chromium oxide. The formation of a nitride layer is confirmed through the presence of nitrogen onto the surface of sintered specimens. The amount of nitrogen for pure 316L stainless steel specimens was 2.82% and was found to be the maximum among all the sintered specimens. The lowest value of 1.93% was observed for 0.5 wt.% titanium added specimens.

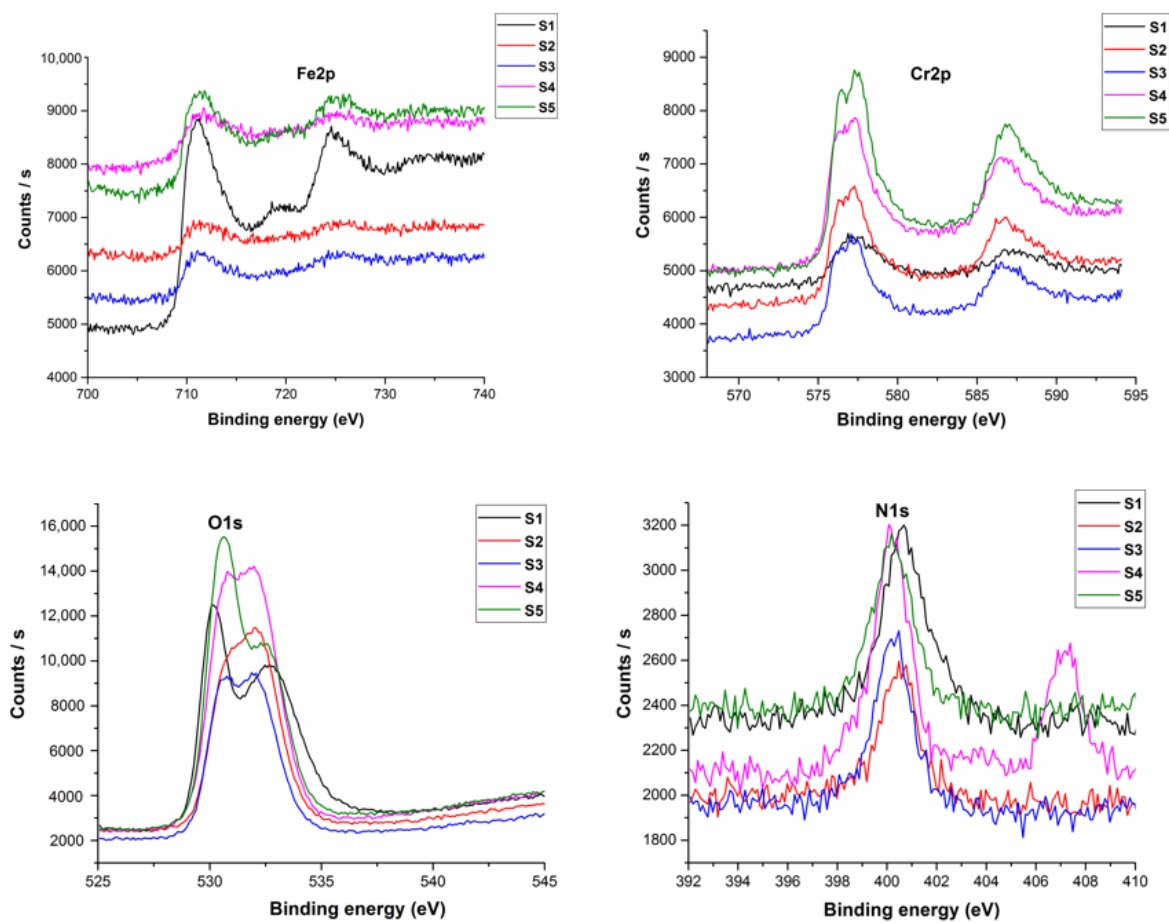


Figure 8. XPS spectra of all specimens.

3.6. Immersion Testing in Artificial Saliva Solution

The immersion testing of sintered specimens was carried out to calculate the weight loss measurements. The specimens were immersed for 28 days in artificial saliva solution to study their corrosion behavior. The weight of the specimens before and after immersion was measured and weight loss calculated. The weight loss measurements for all specimens have been shown in Table 4. The results indicate that nearly all the specimens show good corrosion resistance towards the solution and minimal weight loss is observed for all the specimens. The maximum weight loss of 0.004 g was found for pure 316L SS specimens. The addition of boron and titanium increased corrosion resistance. The maximum corrosion resistance was shown by 2 wt.% titanium added specimens. The passive chromium oxide layer and nitride layer formed on surface of the specimens during sintering resisted in leaching of ions from the solution. This resulted in negligible weight loss during the immersion testing.

Table 4. Weight loss measurements for all samples in artificial saliva solution.

S.No	Alloy	Weight before Immersion	Weight after Immersion	Δm (g)
1	S1	17.310 g	17.306 g	0.004 g
2	S2	18.220 g	18.217 g	0.003 g
3	S3	18.250 g	18.248 g	0.002 g
4	S4	17.240 g	18.237 g	0.003 g
5	S5	18.300 g	18.299 g	0.001 g

The ions released from the sintered specimens were analyzed for their possible concentrations using atomic absorption spectroscopy. A normal human being weighing approximately 70 kg contains

10 mg of nickel in their body, corresponding to concentration of 0.1 ppm and 30 ppm is the critical limit for the cytotoxicity to respond [41]. In this research, the amount of metal ions released are less than the amount of metals in the body. The Table 5 shows the overall results of Fe, Cr and Ni ions released from the sintered specimens. The results indicate that the alloy S1 and S5 released the minimum metal ions, whereas the alloy system S2 and S3 released Ni ions near the critical limit of Ni present in the human body.

Table 5. Concentration of ions released in an artificial saliva solution.

S.No	Alloy	Elements Concentration (ppm)		
		Fe	Cr	Ni
1	S1	0.001	0.000	0.050
2	S2	0.003	0.001	0.090
3	S3	0.009	0.001	0.080
4	S4	0.010	0.003	0.040
5	S5	0.000	0.000	0.050

3.7. In Vitro Cytotoxicity Assessment of Sintered Specimens

In vitro cytotoxicity assessment was calculated by culturing the fibroblast cell line, NIH3T3 on the discs. The cell proliferation was seen on day 3 by using Alamar Blue Assay. The cell viability of the liquid chemicals was assessed using microplate reader absorbance graph. The experiment was performed for 3 days by co-culturing with liquids and the results were then compared with control. The Figure 9 shows the comparison of the results of control for 3 days with the results of deep eutectic solvents for 3 days respectively. The cell proliferation increased with time for deep eutectic solvents and also in contrast to the control. All the specimens indicated increased absorbance as compared to the control.

With five readings from each of the experimental samples, all the analysis was conducted at least twice to get the precise data. Followed by Tukey's post hoc test, a one-way (ANOVA) was performed to check the statistical significant difference between any of the samples. The results having a p-value less than α i.e., < 0.05 were considered to be statistically significant. GraphPad Prism 5.0 software (provided by GraphPad software, San Diego, CA, USA) was used to analyze all the data. All the specimens have their P-value greater than α i.e., > 0.05 , so the difference between the means of the specimens is non-significant, except for S5 which has its P-values being less than α i.e., < 0.05 , so the difference between the means of the metal discs is significant as compared to the control. S5 shows the highest significant difference with P-value of 0.0056 as compared to the control and the standard error of difference is 0.1319. This indicates highest cell proliferation with more antibacterial properties among all the specimens.

The SEM images of the specimens after cytotoxicity assessment have been presented in Figure 10, which clearly show the adhesion of cells to the specimens.

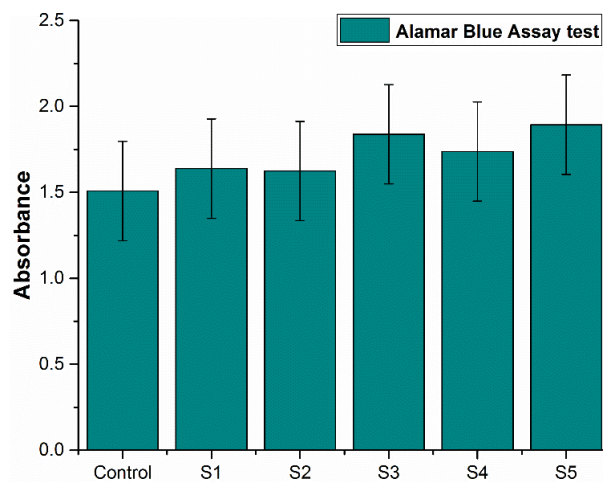


Figure 9. Cytotoxicity assessment of all the specimens.

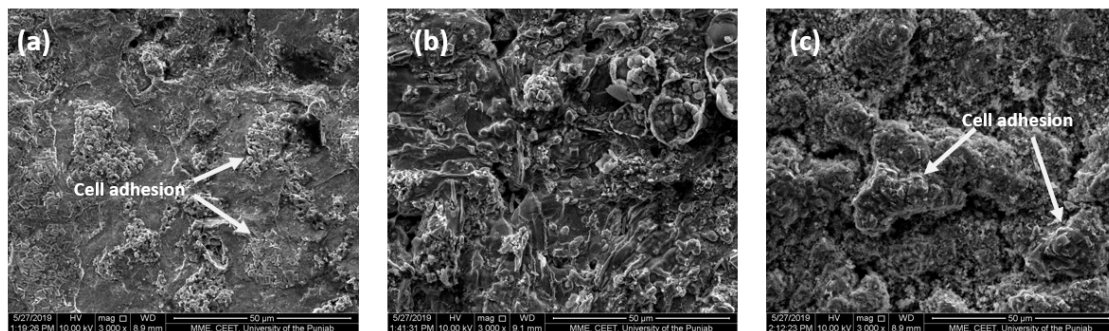


Figure 10. SEM images of specimens after cytotoxicity assessment (a) S1 (b) S3 and (c) S5.

4. Discussion

The 316L stainless steel alloy modified with boron and titanium additions show a notable effect on the performance of the resulting alloy systems. The study demonstrates that a sintering environment and parameters allow better sintering results. These findings open the possibility of producing alloys with tailored physical and mechanical properties. The increase in dwell time up to 8 h favored the nitrogen diffusion into the matrix and formed strong nitrides with iron, boron, titanium and carbon present in the matrix. The XRD and FESEM mapping indicates the presence of nitrogen in the matrix, which helps in increasing the overall performance of the alloy systems. The dwell time of 8 h also supported in development of strong nitride layer on the specimen surface, as indicated by the XPS results. The nitride layer proved to be supportive in retaining nickel and other ions during the immersion testing. It resulted in minimal weight loss of specimens, even after 28 days. The results of atomic absorption spectroscopy revealed that the nickel and other ions were highly reduced. They were within the range of the metal ions present in the human body. These results support the statement that nitride layer has an adequate strength to retain itself and did not allow the chemicals present in the artificial saliva solution to diffuse into the matrix.

The alloying of boron and titanium had a notable effect on the resulting alloy systems. The boron and titanium addition increased the overall strength and corrosion resistance. The micro hardness of the stainless steel alloy system increased up to 366.6 HV for 2 wt.% titanium added specimens. The corrosion resistance was also improved, and minimal weight loss has been observed for 2 wt.% titanium added specimens. The addition of titanium upto 2 wt.% has been found to be suitable in retaining the austenitic structure of the resulting alloy system as indicated by the micro graphs and XRD analysis. The addition also favored the increased compatibility to the living tissues and the results are far better than the pure 316L stainless steel specimens. The SEM results of the specimens clearly

indicate the adhesion of cells on the sample surface, confirming their suitability to be used as implant materials. The addition of titanium although increased the overall performance of the 316L stainless steel but a decrease in the densification behavior has been observed. The densification decreased by increasing the titanium contents and the lowest densification behavior is exhibited by 2 wt.% titanium added specimens.

5. Conclusions

The key conclusion of this research work can be summarized as:

1. 316L stainless steel sintered in nitrogen atmosphere with increased dwell time can help in diffusion of nitrogen into the matrix, thereby forming its respective nitrides as discussed in the XRD and FESEM mapping analysis.
2. The sintering parameters helped in formation of a strong nitride layer onto the surface of the samples, as discussed in the XPS analysis. This layer proved to be helpful in the retention of metal ions during weight loss measurements.
3. The addition of 2 wt.% titanium addition retained the austenitic structure of the resultant alloy systems, which is important in implant manufacturing. Better results were shown by S5 for nearly all the tests, except for density.
4. The corrosion resistance of the alloy systems in artificial saliva solution revealed minimal weight loss with a negligible release of metal ions. This was attributed to the nitrogen which diffused into the matrix and also prepared a strong nitride layer. Both of these results helped in improved corrosion resistance of the alloy systems.
5. The cytotoxicity assessment by MTT assay using fibroblast cells indicated that all the alloy systems studied in this research are non-cytotoxic. The SEM images indicate the cell adhesion to the specimen surface, indicating that cells continue their growth. Specimen S5 with 2 wt.% titanium addition exhibited better results than the others, showing more antibacterial properties and indicating the highest cell proliferation.

Author Contributions: Conceptualization, S.A.; Formal analysis, S.A.; Funding acquisition, R.A.M.; Methodology, S.A.; Project administration, A.M.A.R. and R.A.M.; Resources, S.H., M.H. and N.S.; Supervision, A.M.A.R. and R.A.M.; Writing – original draft, S.A.; Writing – review & editing, Z.B. and A.A.A.A.

Funding: This research was funded by Universitas PERTAMINA – Universiti Teknologi PETRONAS (UP-UTP) International Collaborative Research Fund, cost-centers 015LB0-040 and 015ME0-081 and “The APC was funded by National University of Sciences and Technology (NUST), Islamabad, Pakistan and Universiti Teknologi PETRONAS, Malaysia”.

Acknowledgments: The authors would like to acknowledge Universiti Teknologi PETRONAS, Malaysia for carrying out research and other facilities.

Conflicts of Interest: The authors declare no conflict of interest.

References

1. Wiles, P. The surgery of the osteo-arthritis hip. *Br. J. Surg.* **1958**, *45*, 488–497. [[CrossRef](#)]
2. Wiles, P. The classic: The surgery of the osteo-arthritis hip. *Clin. Orthop. Relat. Res.* **2003**, *417*, 3–16.
3. Lo, K.; Shek, C.H.; Lai, J.; Lai, J.K.L. Recent developments in stainless steels. *Mater. Sci. Eng. R Rep.* **2009**, *65*, 39–104. [[CrossRef](#)]
4. Ali, S.; Rani, A.M.A.; Altaf, K.; Baig, Z. Investigation of Boron addition and compaction pressure on the compactibility, densification and microhardness of 316L Stainless Steel. In *IOP Conference Series: Materials Science and Engineering*; IOP Publishing: Bristol, UK, 2018.
5. Disegi, J.; Eschbach, L. Stainless steel in bone surgery. *Injury* **2000**, *31*, D2–D6. [[CrossRef](#)]
6. Dewidar, M. Influence of processing parameters and sintering atmosphere on the mechanical properties and microstructure of porous 316L stainless steel for possible hard-tissue applications. *Int. J. Mech. Mech. Eng.* **2012**, *12*, 10–24.

7. Ali, S.; Rani, A.M.A.; Altaf, K.; Hussain, P.; Prakash, C.; Hastuty, S.; Rao, T.V.V.L.N.; Subramaniam, K. Investigation of Alloy Composition and Sintering Parameters on the Corrosion Resistance and Microhardness of 316L Stainless Steel Alloy. In *Advances in Manufacturing II*; Springer: Berlin/Heidelberg, Germany, 2019; pp. 532–541.
8. Niinomi, M.; Nakai, M.; Hieda, J. Development of new metallic alloys for biomedical applications. *Acta Biomater.* **2012**, *8*, 3888–3903. [[CrossRef](#)] [[PubMed](#)]
9. Alvarez, K.; Sato, K.; Hyun, S.; Nakajima, H. Fabrication and properties of Lotus-type porous nickel-free stainless steel for biomedical applications. *Mater. Sci. Eng. C* **2008**, *28*, 44–50. [[CrossRef](#)]
10. Thomann, U.I.; Uggowitzer, P.J. Wear–corrosion behavior of biocompatible austenitic stainless steels. *Wear* **2000**, *239*, 48–58. [[CrossRef](#)]
11. Kuroda, D.; Hiromoto, S.; Hanawa, T.; Katada, Y. Corrosion Behavior of Nickel-Free High Nitrogen Austenitic Stainless Steel in Simulated Biological Environments. *Mater. Trans.* **2002**, *43*, 3100–3104. [[CrossRef](#)]
12. Sumita, M.; Hanawa, T.; Teoh, S. Development of nitrogen-containing nickel-free austenitic stainless steels for metallic biomaterials—Review. *Mater. Sci. Eng. C* **2004**, *24*, 753–760. [[CrossRef](#)]
13. Hallab, N. Metal Sensitivity in Patients with Orthopedic Implants. *JCR: J. Clin. Rheumatol.* **2001**, *7*, 215–218. [[CrossRef](#)] [[PubMed](#)]
14. Granchi, D.; Cenni, E.; Tigani, D.; Trisolino, G.; Baldini, N.; Giunti, A. Sensitivity to implant materials in patients with total knee arthroplasties. *Biomaterials* **2008**, *29*, 1494–1500. [[CrossRef](#)] [[PubMed](#)]
15. Vahter, M.; Berglund, M.; Åkesson, A.; Liden, C. Metals and women’s health. *Environ. Res.* **2002**, *88*, 145–155. [[CrossRef](#)] [[PubMed](#)]
16. Yang, K.; Ren, Y. Nickel-free austenitic stainless steels for medical applications. *Sci. Technol. Adv. Mater.* **2010**, *11*, 14105. [[CrossRef](#)] [[PubMed](#)]
17. Foussereau, J.; Laugier, P. Allergic eczemas from metallic foreign bodies. *Trans. St. John’s Hosp. Dermatol. Soc.* **1966**, *52*, 220–225.
18. Gao, X.; He, R.-X.; Yan, S.-G.; Wu, L.-D. Dermatitis Associated with Chromium Following Total Knee Arthroplasty. *J. Arthroplast.* **2011**, *26*, 665.e13–665.e16. [[CrossRef](#)]
19. Beythien, C.; Gutensohn, K.; Fenner, T. Diamond-like carbon coating of coronary stents: Influence on platelet activation, smooth muscle cells and release of metal ions. *Eur. Heart J.* **1998**, *19*, 1947.
20. Menzel, J.; Kirschner, W.; Stein, G. High nitrogen containing Ni-free austenitic steels for medical applications. *ISIJ Int.* **1996**, *36*, 893–900. [[CrossRef](#)]
21. Uggowitzer, P.J.; Magdowski, R.; Speidel, M.O. Nickel free high nitrogen austenitic steels. *ISIJ Int.* **1996**, *36*, 901–908. [[CrossRef](#)]
22. Mirza, A.; King, A.; Troakes, C.; Exley, C. Aluminium in brain tissue in familial Alzheimer’s disease. *J. Trace Elements Med. Boil.* **2017**, *40*, 30–36. [[CrossRef](#)]
23. Mjöberg, B.; Hellquist, E.; Mallmin, H.; Lindh, U. Aluminum, Alzheimer’s disease and bone fragility. *Acta Orthop. Scand.* **1997**, *68*, 511–514. [[CrossRef](#)]
24. Bayon, R.; Igartua, A.; González, J.; De Gopegui, U.R. Influence of the carbon content on the corrosion and tribocorrosion performance of Ti-DLC coatings for biomedical alloys. *Tribol. Int.* **2015**, *88*, 115–125. [[CrossRef](#)]
25. Chen, Q.; Thouas, G.A. Metallic implant biomaterials. *Mater. Sci. Eng. R Rep.* **2015**, *87*, 1–57. [[CrossRef](#)]
26. Manam, N.; Harun, W.; Shri, D.; Ghani, S.; Kurniawan, T.; Ismail, M.H.; Ibrahim, M.; Harun, W.S.W.; Shri, D.N.A.; Ghani, S.A.C. Study of corrosion in biocompatible metals for implants: A review. *J. Alloy. Compd.* **2017**, *701*, 698–715. [[CrossRef](#)]
27. Sulima, I.; Jaworska, L.; Karwan-Baczewska, J. Effect of Boron Sinter-Aid on the Microstructure and Properties of Austenitic Stainless Steel-TIB2 Composites/Wpływ Dodatku Boru Na Mikrostrukturę IW Łaściwosci Kompozytów Stal Austenityczna-TIB2. *Arch. Metall. Mater.* **2015**, *60*, 2619–2624. [[CrossRef](#)]
28. Bayraktaroglu, E.; Gulsoy, H.O.; Gulsoy, N.; Er, O.; Kilic, H. Effect of boron addition on injection molded 316L stainless steel: Mechanical, corrosion properties and in vitro bioactivity. *Bio-Med. Mater. Eng.* **2012**, *22*, 333–349.
29. Szewczyk-Nykiel, A. The effect of the addition of boron on the densification, microstructure and properties of sintered 17-4 PH stainless steel. *Czasopismo Techniczne* **2014**. [[CrossRef](#)]

30. Mishnaevsky, L., Jr.; Levashov, E.; Valiev, R.Z.; Segurado, J.; Sabirov, I.; Enikeev, N.; Prokoshkin, S.; Solov'yov, A.V.; Korotitskiy, A.; Gutmanas, E.; et al. Nanostructured titanium-based materials for medical implants: Modeling and development. *Mater. Sci. Eng. R Rep.* **2014**, *81*, 1–19. [[CrossRef](#)]
31. Correa, D.R.N.; Vicente, F.; Donato, T.; Arana-Chavez, V.; Buzalaf, M.; Grandini, C.R. The effect of the solute on the structure, selected mechanical properties, and biocompatibility of Ti–Zr system alloys for dental applications. *Mater. Sci. Eng. C* **2014**, *34*, 354–359. [[CrossRef](#)]
32. Cordeiro, J.M.; Beline, T.; Ribeiro, A.L.R.; Rangel, E.C.; Da Cruz, N.C.; Landers, R.; Faverani, L.P.; Vaz, L.G.; Fais, L.M.; Vicente, F.B.; et al. Development of binary and ternary titanium alloys for dental implants. *Dent. Mater.* **2017**, *33*, 1244–1257. [[CrossRef](#)] [[PubMed](#)]
33. Shemtov-Yona, K.; Rittel, D. On the mechanical integrity of retrieved dental implants. *J. Mech. Behav. Biomed. Mater.* **2015**, *49*, 290–299. [[CrossRef](#)]
34. Cordeiro, J.M.; Barão, V.A.; Barao, V.A.R. Is there scientific evidence favoring the substitution of commercially pure titanium with titanium alloys for the manufacture of dental implants? *Mater. Sci. Eng. C* **2017**, *71*, 1201–1215. [[CrossRef](#)]
35. Balachandran, G. *High Nitrogen Steels and Stainless Steels—Manufacturing Properties and Applications*; Alpha Science International: Pangbourne, UK, 2004; pp. 40–93.
36. Tsuchiyama, T.; Uchida, H.; Kataoka, K.; Takaki, S. Fabrication of Fine-grained High Nitrogen Austenitic Steels through Mechanical Alloying Treatment. *ISIJ Int.* **2002**, *42*, 1438–1443. [[CrossRef](#)]
37. Kurgan, N. Effects of sintering atmosphere on microstructure and mechanical property of sintered powder metallurgy 316L stainless steel. *Mater. Des.* **2013**, *52*, 995–998. [[CrossRef](#)]
38. Saller, G.; Spiradek-Hahn, K.; Scheu, C.; Clemens, H. Microstructural evolution of Cr–Mn–N austenitic steels during cold work hardening. *Mater. Sci. Eng. A* **2006**, *427*, 246–254. [[CrossRef](#)]
39. Chao, Z.; Yaomu, X.; Chufeng, L.; Conghua, L. The effect of mucin, fibrinogen and IgG on the corrosion behavior of Ni–Ti alloy and stainless steel. *Biometals* **2017**, *30*, 367–377. [[CrossRef](#)]
40. Hussein, M.A.; Yilbas, B.; Kumar, A.M.; Drew, R.; Al-Aqeeli, N. Influence of Laser Nitriding on the Surface and Corrosion Properties of Ti-20Nb-13Zr Alloy in Artificial Saliva for Dental Applications. *J. Mater. Eng. Perform.* **2018**, *27*, 4655–4664. [[CrossRef](#)]
41. Das, K.K.; Das, S.N.; Dhundasi, S.A. Nickel, its adverse health effects & oxidative stress. *Indian J. Med. Res.* **2008**, *128*, 412.



© 2019 by the authors. Licensee MDPI, Basel, Switzerland. This article is an open access article distributed under the terms and conditions of the Creative Commons Attribution (CC BY) license (<http://creativecommons.org/licenses/by/4.0/>).